Heliyon 9 (2023) e15580

Contents lists available at ScienceDirect

Heliyon

journal homepage: www.cell.com/heliyon

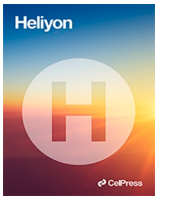

Research article

Design of hydrophobic polyurethane–magnetite iron oxide-titanium dioxide nanocomposites for oil-water separation

Asma Khandan Barani [a], Ghodratollah Roudini [b], Farahnaz Barahuie [c,*], Siti Ujila Binti Masuri [d]

[a] Nanotechnology Research Institute, Faculty of Engineering, University of Sistan and Baluchestan, Zahedan, Iran
[b] Department of Materials Engineering, Faculty of Engineering, University of Sistan and Baluchestan, Zahedan, Iran
[c] Faculty of Industry & Mining (Khash), University of Sistan and Baluchestan, Zahedan, Iran
[d] Department of Mechanical and Manufacturing Engineering, Faculty of Engineering, University Putra Malaysia, Serdang, Malaysia

ARTICLE INFO

Keywords:
Nanocomposite
Polyurethane
Hydrophobicity
Iron oxide nanoparticle
Oil-water separation
Titanium dioxide nanoparticle

ABSTRACT

Efficacious oil-water separation has become a global challenge owing to regular oil spillage accidents and escalating industrial oily wastewater. In this study, we synthesized titanium dioxide and magnetite iron oxide nanoparticles to use as a precursor for the production of the nanocomposites. Hydrophobic nanocomposites were fabricated using polyurethane, hematite and magnetite iron oxide nanoparticles, and titanium dioxide nanoparticles through a sol-gel process. The formation of the obtained nanocomposites was confirmed by X-ray diffraction (XRD), Fourier transform infrared spectroscopy (FTIR), and scanning electron microscopy (SEM) analyses. In addition, the thermogravimetric and differential thermogravimetric (TGA/DTG) and BET surface area results exhibited enhanced thermal stability of the optimized nanocomposite which displayed mesoporous type materials feature with high porosity. Furthermore, the obtained outcomes demonstrated that the distribution of nanoparticles into a polymer matrix had a significant impact on enhancing superhydrophobicity and the separation efficiency against sunflower oil. Seeing the water contact angle of the nanocomposite-coated filter paper was about 157° compared to 0° for the uncoated filter paper and endowed separation efficiency of almost 90% for 5 consecutive cycles. Thereby, these nanocomposites could be an ideal candidate for self-cleaning surfaces and oil-polluted water purification.

1. Introduction

Sustainable clean water supply has emerged as one of the greatest issues facing the world since rapid industrial development and frequent crude oil leakages have led to the generation of large amounts of oily wastewater. These indecomposable waste oils not only threatened the ecosystem but also greatly aggravated water scarcity [1–3]. Conventional separation methods due to the high stability of oil–water mixtures, have limited effectiveness in treating oil-water mixtures. Therefore, it is urgent to develop new technology and advanced materials which efficiently separate oil/water mixtures [4–6].

Nanotechnology is cutting-edge science, having the potential to curb challenges confronted in the existing water treatment crisis. It has the aptitude to cater the solutions related to water pollution detection, remediation, and purification with the technological use of

* Corresponding author.
E-mail address: farahnaz.barahuie@eng.usb.ac.ir (F. Barahuie).

https://doi.org/10.1016/j.heliyon.2023.e15580
Received 24 November 2022; Received in revised form 12 April 2023; Accepted 14 April 2023
Available online 20 April 2023

nanomaterials. Engineered nanocomposites with special wettability, particularly hydrophobic-oleophilic materials are an appealing choice for various applications [7–9].

Diverse strategies including chemical vapor deposition, phase separation, spray coating, ink-jet printing, and sol-gel method, have been utilized to make hydrophobic surfaces on variant substrates. The hydrophobic surfaces with high water contact angles and low sliding angles features have been broadly sought after due to the huge potential in various applications such as transparent and antireflective surfaces, fluidic drag reduction, anti-fog and anti-freezing to windows and antennas, self-cleaning and anti-biofouling surfaces, and oil-water separation [10,11].

Polyurethane (PU)-based nanocomposites are the most commonly used and beneficial coating materials that can be tailored for versatile applications, particularly in self-cleaning surfaces and oil-water separation fields. The flexibility in the variety of macro diols, di-isocyanates, and chain extenders in PU provide broad relevance of PU coatings with a widespread scope of physical, adhesion, and mechanical properties [12–15].

Currently, there is a growing interest in nanoparticles of metal oxides. The excellent performance of titanium dioxide (TiO_2) nanoparticles in a wide range of disciplines such as heterogeneous photo-catalyst, water treatment, self-cleaning surfaces, food and pharmaceutics, UV blockers, and white pigment in paints, which are attributed to their good physical and chemical properties [16–18]. Tremendous sensitivity towards ammonia gas, high electrical conductivity, and good thermal stability of polypyrrole-silver-TiO_2 [19], polyaniline-cerium- TiO_2 [20], and polyaniline phenothiazine-TiO_2 [21] nanocomposites, the great self-cleaning activity of acrylic-TiO_2 nanocomposite [22], and appropriate electrical, thermal and mechanical properties of poly butyl methacrylate-neodymium-TiO_2 nanocomposites [23] were attributable to the existence of TiO_2 nanoparticles in these nanocomposites.

The attention of researchers is focused on magnetite iron oxide nanoparticles (Fe_3O_4), as a kind of spinel ferrite with stable magnetic permeability and superparamagnetism, that have versatile properties and possible applications in magnetic resonance imaging, data storage, biological labels for anticancer therapy, electromagnetic interference shielding, wastewater treatment and oil recovery, and catalysis [24–26]. The presence of Fe_3O_4 nanoparticles in fabricated polyvinylidene fluoride-Fe_3O_4 nanocomposite by electrospinning technique [27], prepared poly anthranilic acid-Fe_3O_4 nanocomposite via in situ chemical oxidative polymerization process [28], and produced polymer-Fe_3O_4@graphene nanocomposite using DLF procedure [29], enhanced electrical, magnetic, and mechanical properties of the nanocomposites.

Hematite iron oxide (Fe_2O_3) nanoparticle is of particular curiosity owing to its outstanding electrical and magnetic properties, low cost, and environmentally friendly features. By virtue of its fascinating structural, suitable surface, thermal, and chemical characteristics, has been widely explored in pigments, water treatment, biomedical (drug delivery, stimuli-responsive stents, and magnetic resonance imaging), lithium-ion battery, storage media, sensing, and photochemical applications [30,31]. The Fe_2O_3 nanoparticles in Fe_2O_3-poly-aminoanthraquinone@BiVO nanocomposite boosted the water-splitting efficiency by accelerating the proton-coupled electron transfer process [32].

Here, we synthesized TiO_2 and Fe_3O_4 nanoparticles first to use them as a precursor for the preparation of nanocomposites. Since there was no report on polyurethane-iron oxide-TiO_2 nanocomposite in literature, this study aimed to fabricate hydrophobic nanocomposites using synthesized TiO_2 and Fe_3O_4 nanoparticles, polyurethane pellets, and Fe_2O_3 nanoparticles. Fe_3O_4 and Fe_2O_3 nanoparticles were selected due to their good magnetic properties which improve hydrophobic property and TiO_2 nanoparticle was chosen due to its hydrophobic feature. The newly formed nanocomposites were characterized for their structural, surface morphology, and thermal stability. The hydrophobicity, the performance of the nanocomposites in oil-water separation, separation efficiency, and reusability were evaluated.

2. Experimental

2.1. Materials

Ferrous chloride tetrahydrate ($FeCl_2 \cdot 4H_2O$, 98%), ferric chloride hexahydrate ($FeCl_3 \cdot 6H_2O$, 99%) , hydrochloric acid (HCl, 37%), ethanol, and N, N-dimethylformamide (DMF) were acquired from Merck, Germany. Sodium hydroxide (NaOH) was purchased from Friedemann Schmidt (Parkwood, WA, USA). Titanium(IV) butoxide (Ti(*O*-Bu)4, 98%), ACROS Organics, Geel, Belgium. Polyurethane (PU) pellets ($C_{17}H_{16}N_2O_4$, molecular weight = 312 g/mol, density = 1.18 g/cm^3) were gained from Lubrizol Advanced Material, Korea. Deionized water was used in the experiments. Sunflower oil was obtained from the local market.

2.2. Preparation of nanoparticles and nanocomposites

2.2.1. Synthesis of TiO_2 nanoparticles and Fe_3O_4 nanoparticles

TiO_2 nanoparticles were synthesized through an established sol-hydrothermal method [33] and the co-precipitation technique was used to prepare Fe_3O_4 nanoparticles as previously reported [34].

2.2.2. Synthesis of PU-Fe_3O_4- TiO_2 nanocomposite

An appropriate amount of PU pellets was dissolved in DMF under vigorous stirring at a temperature of 50°C. Then, the synthesized TiO_2 and Fe_3O_4 nanoparticles were added in two conical flasks which contain DMF and the samples were sonicated for 1 h. After the dispersion of the nanoparticles, the dispersed nanoparticles were slowly added to the PU solution and the mixture was stirred for 6 h at 40 °C. Finally, the mixture was dried in the oven at 60 °C for 48 h. The amount of Fe_3O_4 and TiO_2 nanoparticles was varied and the samples are referred to as PUMNPTNP1, PUMNPTNP2, and PUMNPTNP3 (Table 1 and Fig. 1).

Table 1
PU, Fe_3O_4 nanoparticles, and TiO_2 nanoparticles compositions used for the preparation of the PUMNPTNP nanocomposites.

Nanocomposite	PU (g)	Fe_3O_4 nanoparticles (g)	TiO_2 nanoparticles (g)
PUMNPTNP1	1	0.5	0.5
PUMNPTNP2	1	1	0.5
PUMNPTNP3	1	1	1

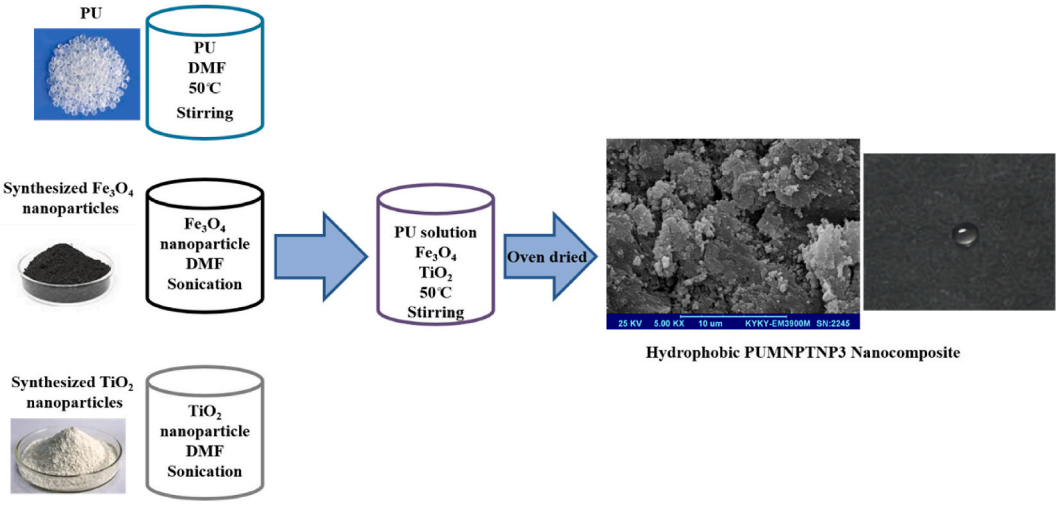

Fig. 1. Schematic diagram of PU-Fe_3O_4–TiO_2 nanocomposite preparation.

Table 2
PU, TiO_2 nanoparticles, and Fe_2O_3 nanoparticles compositions used for the preparation of the PUHNPTNP nanocomposites.

Nanocomposite	PU (g)	TiO_2 nanoparticles (g)	Fe_2O_3 nanoparticles (g)
PUHNPTNP1	1	0.5	0.5
PUHNPTNP2	1	1	1

2.2.3. Synthesis of PU-Fe_2O_3- TiO_2 nanocomposite

The PU-Fe_2O_3–TiO_2 nanocomposites nanocomposites were fabricated by a sol-gel process. First, Fe_2O_3 and synthesized TiO_2 nanoparticles were dispersed in DMF (15 mL) under ultrasonic for 1 h. Meanwhile, PU pellets were dissolved in DMF (25 mL) at a temperature of 50 °C with stirring for 2 h. Then the TiO_2 and Fe_2O_3 suspensions were gently poured into a PU solution and the mixture was stirred for 6 h at 40 °C. The resulting slurry was then oven-dried at 60 °C for 48 h. The samples containing different amounts of TiO_2 and Fe_2O_3 nanoparticles were labeled as PUHNPTNP1 and PUHNPTNP2 (Table 2).

2.3. Characterization

Fourier transform infrared spectra of the samples were recorded over the range of 400–4000 cm^{-1} on a Thermo Nicolet FTIR (AEM, Madison, WI, USA) with 4 cm^{-1} resolution using the potassium bromide disc method. The morphologies of Fe_3O_4 and TiO_2 nanoparticles, and the nanocomposite were observed by scanning electron microscopy (SEM, JEOL, JSM-7610F, Japan). Surface characterization of the nanocomposite was carried out using the nitrogen gas adsorption–desorption technique at 77 K, using a Micromeritics ASAP 2000 (Norcross, GA, USA). The composition and crystalline structure of the materials were analyzed via an XRD-6000 diffractometer (Shimadzu, Tokyo, Japan) by studying the angles from 5 to 70° using CuKα radiation ($\lambda = 1.5406°$ A) at 40 kV and 30 mA. Thermogravimetric and differential thermogravimetric analyses (TGA/DTG) were carried out using a Mettler-Toledo instrument (Greifensee, Switzerland) in the range of 20–1000 °C at a heating rate of 10 °C/min under a nitrogen atmosphere to determine the thermal behavior of the nanocomposite.

2.4. Preparation of oil-water emulsion

The oil-water emulsion was prepared using commercial sunflower oil and distilled water following vigorous mechanical stirring of the mixture for 25 min. The oil concentration of the emulsion was 150 g/L.

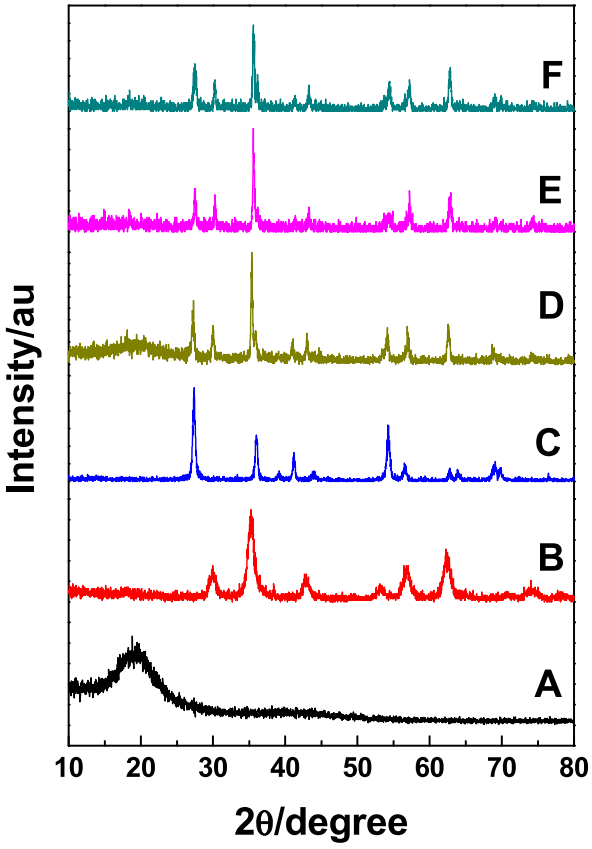

Fig. 2. X-ray diffraction patterns for PU (A), Fe_3O_4 nanoparticles (B), TiO_2 nanoparticles (C), and PUMNPTNP1 nanocomposite (D), PUMNPTNP2 nanocomposite (E), and PUMNPTNP3 nanocomposite(F).

2.5. Coating of the nanocomposites on filter paper

The obtained sol-gel nanocomposite solution was kept in the oven for 24 h and after evaporation of some amount of solvent, we added the nanocomposite solution through ink injection on the filter paper with the pore size of 20–25 μm. It was then allowed to dry in the oven for 8 h at 60 °C.

3. Results and discussion

3.1. X-ray diffraction

The XRD patterns of PU, Fe3O4 nanoparticles, Fe2O3 nanoparticles, TiO2 nanoparticles, PUMNPTNP1 nanocomposite, PUMNPTNP2 nanocomposite, PUMNPTNP3 nanocomposite, PUHNPTNP1 nanocomposite, and PUHNPTNP2 nanocomposite were shown in Figs. 2 and 3.

The XRD pattern of PU (Figs. 2A and 3A) revealed the broad peak at around $2\theta = 20.3^{\circ}$ which indicates a typical pattern for a low crystalline material [35].

In Fig. 2B, the characteristic diffraction peaks of synthesized Fe_3O_4 nanoparticles were marked by their indices (220), (311), (400), (422), (511), and (440) which proved the formation of cubic inverse spinal structure of Fe_3O_4 nanoparticles [36]. The crystallite size was calculated using the Debye -Scherrer's equation $\left(D = \frac{K\lambda}{\beta \cos\theta}\right)$, where D was the average particle size, K was the Scherrer constant (0.9), λ was the XRD wavelength (0.15418 nm), β was the peak width of half maximum intensity, and θ was the Bragg diffraction angle. Thus the mean grain size was obtained 29 nm [37].

The diffractogram of the fabricated TiO_2 (Figs. 2C and 3C) exhibited diffraction peaks at (110), (101), (200), (111), (210), (211), (220), (002), (310), (301) and (112) crystallographic planes, which agree with those reported for the standard crystal structure of rutile (TiO_2). The crystal size (D) of the TiO_2 could be determined through Debye -Scherrer's equation and was around 31 nm [38,39].

As shown in Fig. 2D, the broad diffraction peak of pristine PU, typical diffraction peaks of Fe_3O_4, and characteristic bands of TiO_2 nanoparticles were indicated the presence of polymer, Fe_3O_4, and TiO_2 nanoparticles in the PUMNPTNP1 nanocomposite. It was observed that the intensity of Fe_3O_4 and TiO_2 nanoparticles peaks was increased by increasing the amount of Fe_3O_4 and TiO_2

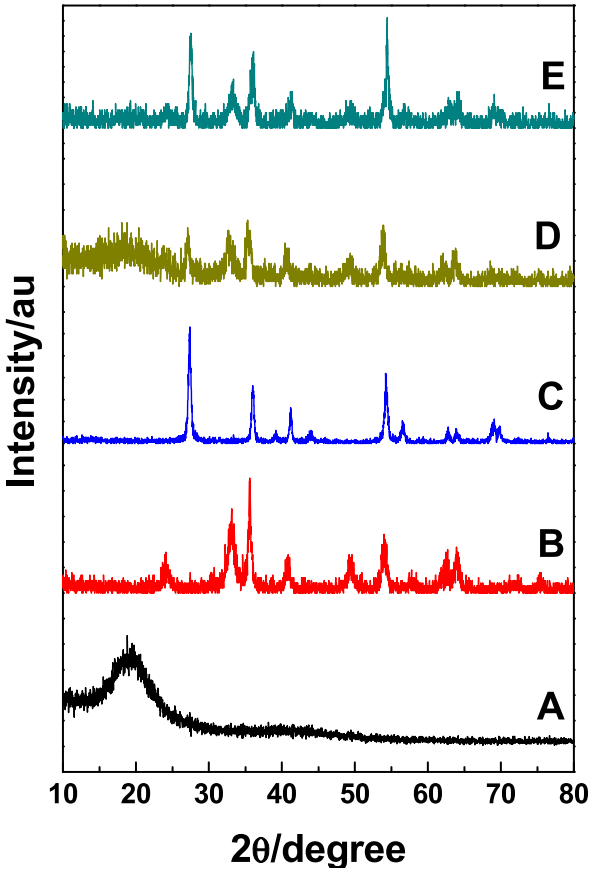

Fig. 3. X-ray diffraction patterns for PU (A), Fe_2O_3 nanoparticles (B), TiO_2 nanoparticles (C), and PUHNPTNP1 nanocomposite (D), and PUHNPTNP2 nanocomposite (E).

nanoparticles loaded on PUMNPTNP2 nanocomposite (Fig. 2E), and PUMNPTNP3 nanocomposite (Fig. 2F), respectively.

In the case of Fe_2O_3 nanoparticles (Fig. 3B), the distinct peaks at 24.11°, 33.12°, 35.26°, 40.72°, 49.36°, 53.74°, 57.81°, 62.46°, and 63.86°, could be assigned to (012), (104), (110), (113), (024), (116), (018), (214), and (300) planes, which are consistent with the standard pattern of Fe_2O_3 (JCPDS, No. 86-0550) [40].

These characteristic peaks of PU, Fe_2O_3 nanoparticles, and TiO_2 nanoparticles were observed in PUHNPTNP1 nanocomposite (Fig. 3D), and the intensity of Fe_2O_3 and TiO_2 nanoparticles peaks was raised by the increasing amount of Fe_2O_3 nanoparticles and TiO_2 nanoparticles loaded on PUHNPTNP2 nanocomposite (Fig. 3E).

3.2. FTIR spectroscopy

Figs. 4 and 5 displayed the FTIR spectra of PU, Fe_3O_4 nanoparticles, Fe_2O_3 nanoparticles, TiO_2 nanoparticles, PUMNPTNP1 nanocomposite, PUMNPTNP2 nanocomposite, PUMNPTNP3 nanocomposite, PUHNPTNP1 nanocomposite, and PUHNPTNP2 nanocomposite. The PU was used as a reference polymer to elucidate the successful preparation of the nanocomposites.

In the FTIR spectrum of pure PU (Figs. 4A and 5A), the stretching vibration of N–H appeared at 3295 cm^{-1} and the peaks at 2926 cm^{-1} and 2866 cm^{-1} were related to the symmetric and asymmetric stretching vibration of CH_2 groups. The band at 1712 cm^{-1} is attributed to the C=O group of the urethane bond, while the NH out-of-plane bending vibration and C–N stretching vibration, were recorded at 1512 cm^{-1} and 1307 cm^{-1}. The peaks at 1594 cm^{-1} and 1435 cm^{-1} were due to the stretching vibration of C=C, and the characteristic band at 1220 cm^{-1} was ascribed to the C–O stretching vibration [35,41].

In the FTIR spectrum of synthesized Fe_3O_4 nanoparticles (Fig. 4B), the band at 541 cm^{-1} was defined as typical stretching vibration of Fe–O [37] and it was shifted to the higher wave numbers in the nanocomposites due to the interaction of Fe_3O_4 nanoparticles with PU.

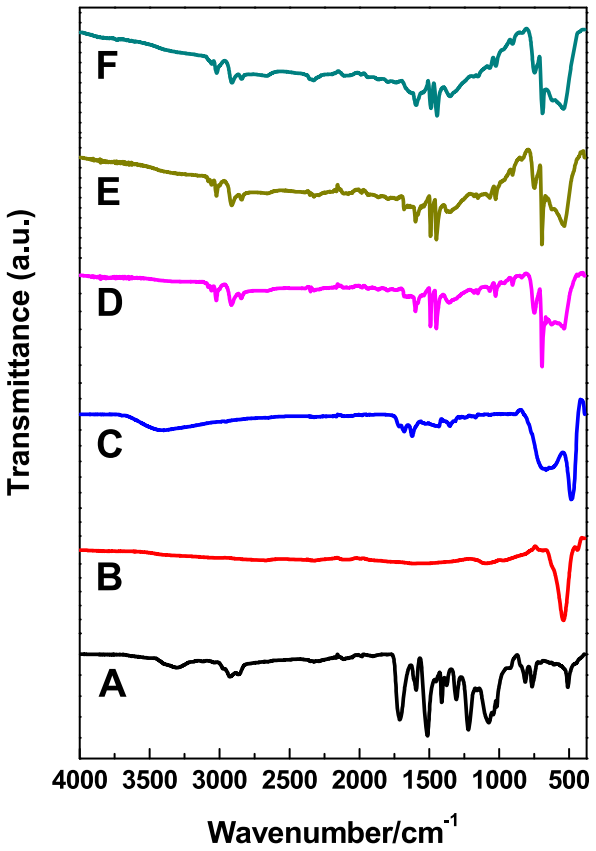

Fig. 4. FTIR spectrums for PU (A), Fe_3O_4 nanoparticles (B), TiO_2 nanoparticles (C), and PUMNPTNP1 nanocomposite (D), PUMNPTNP2 nanocomposite (E), and PUMNPTNP3 nanocomposite (F).

In the FTIR spectrum of synthesized TiO_2 nanoparticles (Figs. 4C and 5C), a distinct peak at 485-685 cm^{-1} was regarded with the stretching and bending modes of Ti–O groups which are consistent with the previous reports in the literature for the rutile phase of TiO2 nanoparticles [42]. This band was shifted to the higher frequencies in the nanocomposites as a result of the interaction between PU and TiO_2 nanoparticles.

In the FTIR spectrum of Fe_2O_3 nanoparticles (Fig. 5B), the vibrational bands of Fe–O were recorded at 434 cm^{-1} and 520 cm^{-1} [43] and these peaks slightly shifted in the nanocomposites.

For the nanocomposites (Figs. 4D and E, and 5D–F), due to the interaction between Fe_3O_4, Fe_2O_3, and TiO_2 with PU, the typical peak of C=O functional group, NH out of plane bending vibration, C–O stretching vibration, and the stretching vibration of N–H were observed with low intensity and shifted to the lower frequencies in the presence of these nanoparticles. There was an interaction between the oxygen of the Fe_3O_4, Fe_2O_3, and TiO_2 nanoparticles with the NH of the urethane bond forming complexes. This was probably due to the formation of hydrogen bonding between PU with the nanoparticles and the hydrogen bonding enhances the adhesion between the nanoparticles and the polymer matrix.

3.3. Surface morphology and N2 adsorption-desorption analysis

The morphologies of synthesized Fe_3O_4 nanoparticles, PUMNPTNP3 nanocomposite, and prepared TiO_2 nanoparticles were observed by scanning electron microscope (SEM). Fig. 6(A–C) indicated that the synthesized TiO_2 nanoparticles had a spherical shape with a mean size of 31 nm. The SEM images of the prepared Fe_3O_4 nanoparticles were depicted in Fig. 6(D–F). The roughly monodispersed spherical particles with an average size of 29 nm were observed. In Fig. 6(G–I), it can be seen that by the distribution of Fe_3O_4 and TiO_2 nanoparticles to the PU matrix to form polymer nanocomposite, the PU density and surface roughness were increased. Besides, irregular and porous surfaces in PUMNPTNP3 nanocomposite were perceived which was ascribed to the dispersion of Fe_3O_4 and TiO_2 nanoparticles and strong interface adhesion in the PU matrix.

The surface area and porosity of the PUMNPTNP3 nanocomposite were analyzed using N_2 adsorption-desorption isotherms (Figs. 7A and 7B). According to Brunauer-Emmett-Teller, type IV isotherm was detected for the PUMNPTNP3 nanocomposite, indicating the formation of a mesoporous structure [44]. Additionally, it could be observed from Fig. 7A that the N_2 uptake gradually rose

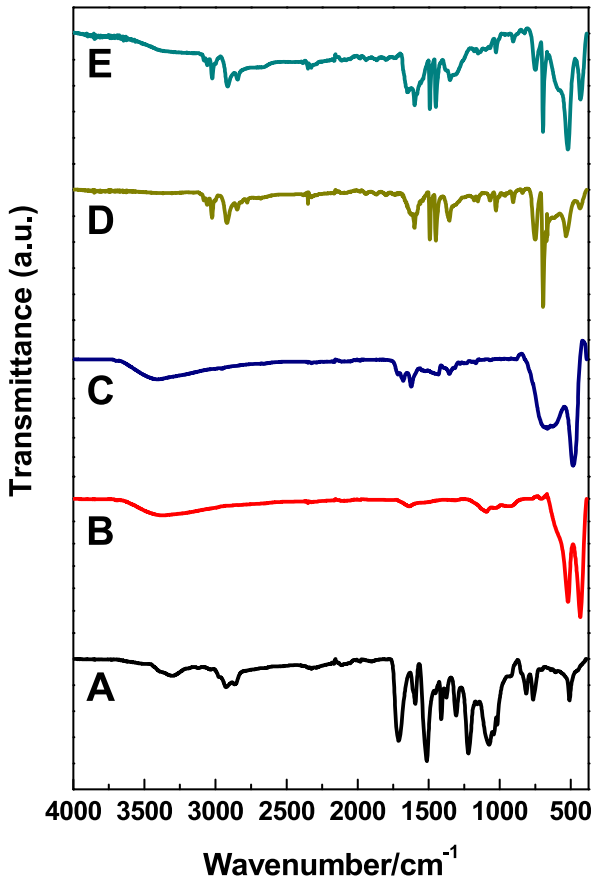

Fig. 5. FTIR spectrums for PU (A), Fe_2O_3 nanoparticles (B), TiO_2 nanoparticles (C), and PUHNPTNP1 nanocomposite (D), and PUHNPTNP2 nanocomposite (E).

with the growth of the relative pressure and the BET surface of the nanocomposite was around 45.0 m^2/g. Even more, the pore volume and average pore diameter of the PUMNPTNP3 nanocomposite which were obtained from Barret–Joyner–Halenda (BJH) desorption pore size distribution plot were 1.8 cm^3/g and 326 nm, respectively (Fig. 7B).

3.4. Thermal analysis

In order to verify the formation of the PUMNPTNP3 nanocomposite and investigate its thermal stability, the thermal behavior of the nanocomposite was measured via thermogravimetric and differential thermogravimetric (TGA/DTG) analyses. Fig. 8 demonstrated that the decomposition of PUMNPTNP3 nanocomposite progressed through two major stages of weight loss, occurring at temperature maxima of 319.9 °C and 406.6 °C, respectively. The two steps of weight loss were attributed to the thermodynamical incompatibility of the soft and hard domains in PU. The first step of weight loss was due to the depolycondensation reaction of PU to produce precursors such as polyols and isocyanates, then isocyanates were dimerized to form carbodiimides, accompanied by the volatilization of small molecules such as carbon oxides, alcohols, and aldehydes (degradation of the soft domain in PU). Besides, the second step was associated with the decomposition of the substituted urea resulting from the reaction of carbodiimides with water or alcohol (degradation of the hard domain in PU). However, in the prior studies were reported that pure PU was decomposed in two steps at the maximum temperature of 327 °C and 370 °C, respectively. Therefore, it can be concluded from the above results that the addition of Fe_3O_4 and TiO_2 nanoparticles into the PU matrix enhanced the thermal stability of the PU in the nanocomposite [39,45].

3.5. Surface wettability and oil-water separation performance of the nanocomposite coated filter paper

The surface wetting properties of the modified and unmodified filter papers in the air and ambient temperature were examined (Fig. 9). The deionized water was randomly dropped on the surfaces of the modified and unmodified filter papers and the water contact angle was measured by selecting several points of the same sample arbitrarily. The water droplet quickly penetrated into the unmodified filter paper and the contact angle was 0°. However, for the PUMNPTNP3 nanocomposite-coated filter paper, the shape of

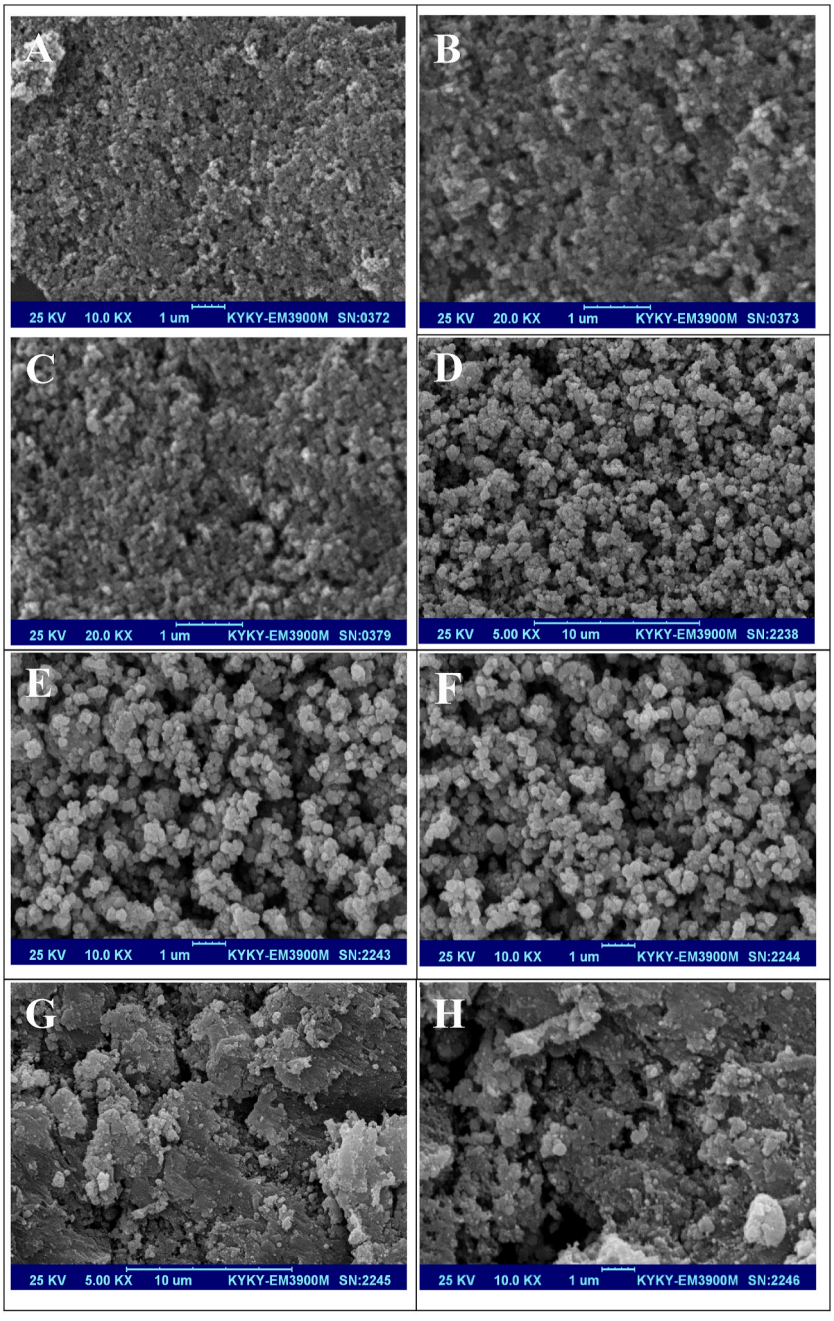

(caption on next page)

Fig. 6. SEM images of TiO_2 nanoparticles (A–C), Fe_3O_4 nanoparticles (D–F), and PUMNPTNP3nanocomposite (G–I).

droplets remained unchanged and the water contact angle reached around 157° and remained substantially constant.

Next, the oil−water separation test was carried out on a device as shown in Fig. 9 to further verify the function of the nanocomposite hydrophobicity. The nanocomposite-coated filter paper was placed into the funnel. The artificial oily wastewater was poured through a funnel with a nanocomposite-coated filter paper inserted. In the separation process, oil permeated through the coated filter paper and dripped into the below-collecting beaker (Fig. 9), but the water was repelled and stayed above the coated filter paper. This phenomenon divulged that these nanocomposites have hydrophobic features and the composites coating can separate oil−water mixtures.

To evaluate the separation performance for nanofilter, the amount of feed and passed oil after the separation process was recorded and calculated using the following equation

$$\gamma = \frac{m_1}{m_0} \times 100$$

where γ is the separation efficiency, m_1 is the mass of permeate and m_0 presents the mass of feed oil during the separation process [46]. To investigate the cycling stability of the proposed nanofilter, the separation process was repeated over 5 cycles. To confirm the accuracy of the reusability test, the prepared nanofilter was dried under a vacuum oven at 60 °C for 3 h.

However, all of these results revealed that the PUMNPTNP3 nanocomposite had the greatest hydrophobic property among the

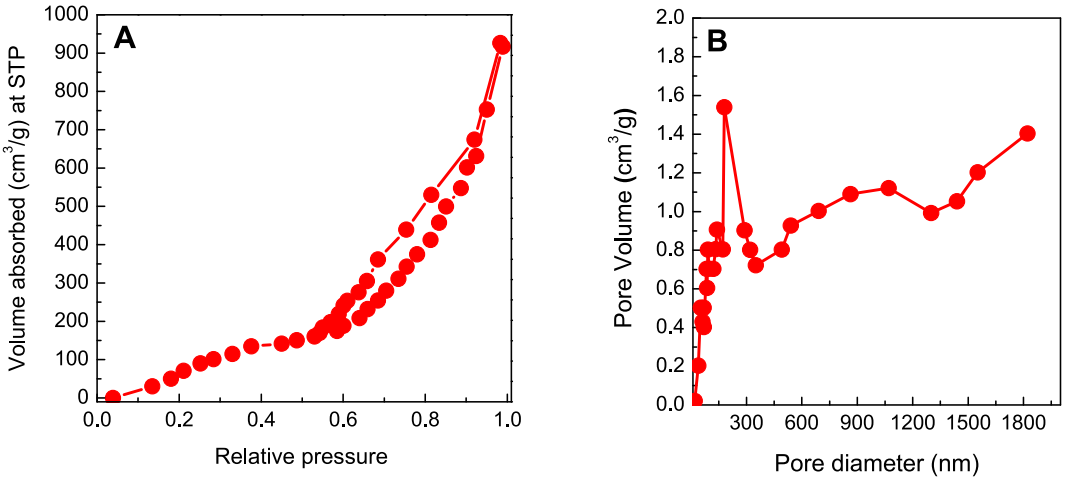

Fig. 7. N_2 adsorption–desorption isotherms (A) and Barret-Joyner-Halenda method pore size distribution (B) of PUMNPTNP3 nanocomposite.

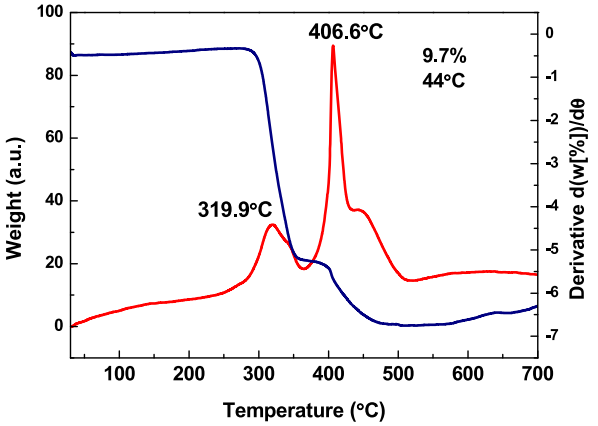

Fig. 8. TGA/DTG curves of PUMNPTNP3 nanocomposite.

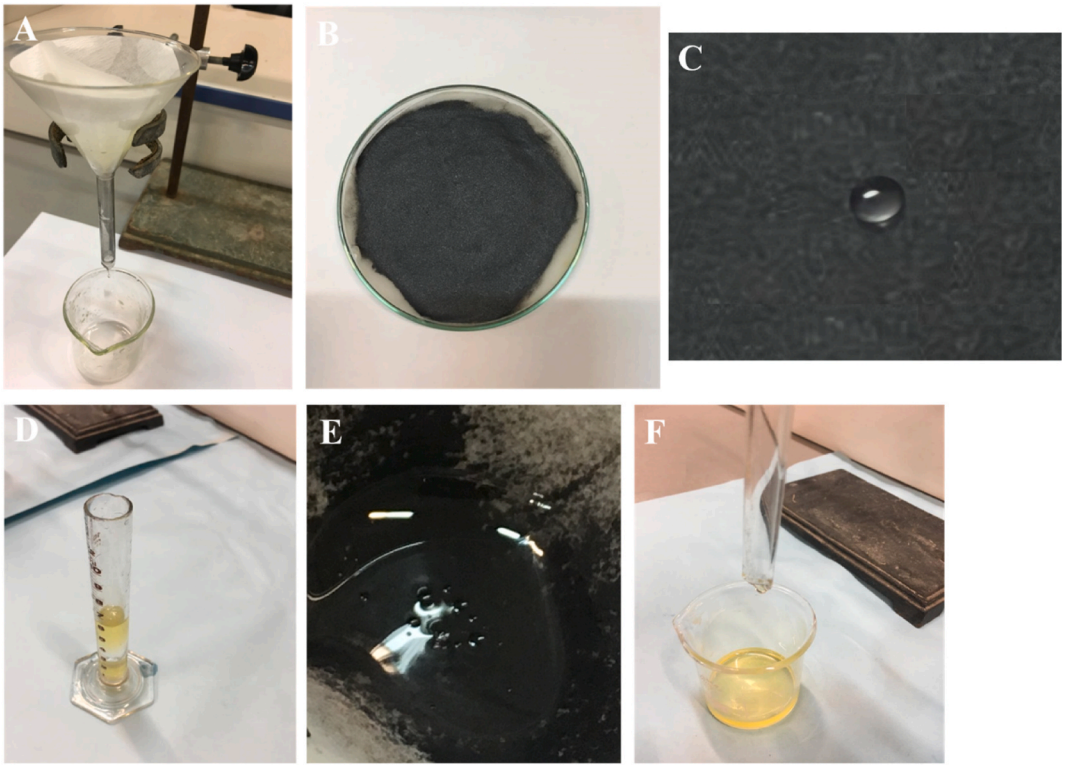

Fig. 9. Photographs of surface wettability of unmodified (A) and modified (B and C) filter papers and oil-water separation set-up of modified filter paper (D–F).

nanocomposites with around 90% separation efficiency which could be related to the high amount of Fe_3O_4 nanoparticles with superior magnetic features and TiO_2 nanoparticles with good hydrophobic properties in PUMNPTNP3 nanocomposite. Hence, this makes PUMNPTNP3 nanocomposite, a unique and promising hydrophobic material for practical applications.

3.6. Discussions

PU-based materials with hydrophobic-oleophilic properties have been reported for oil−water separation. PU is a commercially available material suitable for oil-water separation applications after appropriate modifications [47–51]. As the wettability is controlled by the surface roughness and structure, thus the hydrophobic and magnetic materials (TiO_2 and Fe_3O_4 nanoparticles) introduced hydrophobic properties in the nanocomposite by modification of surface roughness and structure of the nanocomposite (Fig. 6G–I). TiO_2 and Fe_3O_4 nanoparticles showed hydrophobicity with a large surface area and were often-desired modifiers with low surface energy and stability that improved the surface hydrophobicity in a controllable manner. For instance, a surface roughness induced superhydrophobicity of graphene nanocomposite was reported by incorporating Fe_3O_4 nanoparticles and TiO_2 nanoparticles induced superhydrophobicity in cotton. TiO_2 and Fe_3O_4 nanoparticles were employed as a filler to PU matrix by the strong dipole–dipole attractions, changed the surface roughness, and significantly improved the surface durability towards drop impact.

Likewise [46,52–55], the oil trapped between the nanocomposite pores augmented water repellency and furthered water rejection. The hydrophobic PUMNPTNP3 nanocomposite offered enormous space for absorption and a bigger specific surface area to allow oil absorptivity.

The PUMNPTNP3 nanocomposite separation capacity was compared with previous studies (Table 3). Various materials like polymers, metal oxide nanoparticles, carbon materials, and metal organic-frameworks have been applied to get desirable surface wettability for oily water treatment. Surely, the Table data expressed that the newly accomplished nanocomposite has shown a good performance in sunflower oil–water separation among peers.

Table 3
Recent advancements in super-wetting materials in oil-water emulsion separation.

Nanocomposite/composite	Method	Special wettability	Contact angle	Oil-water separation efficiency	Emulsified oils	References
Polystyrene-Fe_3O_4	Electrospinning	Superhydrophobic	162.0°	95.00 92.00	Olive oil, Sesame oil	[46]
Polydopamine-polypyrrole-polyaniline-Fe-stearic acid-polyurethane	Dip-coating two-step	Superhydrophobic	164.0°	99.00	–	[51]
Polyvinyl alcohol cross-linked tannic acid-magnetic TiO_2-MXene	Magnetic self-assembly	Superhydrophilic	–	99.85	–	[56]
Polybutylene succinate nanofiber	Solution blow spinning	Superhydrophobic	–	98.10–99.50	Soybean oil, diesel, gasoline mineral oil, silicon oil	[57]
CaCO3 coated-stainless steel meshe	Biomineralization	Superhydrophilic	161.0°	98.50	–	[58]
Mg-silicate@glass fiber fabric	Universal epitaxial growth	Superhydrophilic	156.3°	99.50	Industrial oily sewage	[59]
Bacterial cellulose-cellulose nanocrystals	Immersion	Superhydrophilic	–	97.60	–	[60]
Sugarcane bagasse-nanofiber	Electrospinning	Superhydrophilic	–	99.60	–	[61]
Co_3O_4-stainless steel mesh	Co-precipitation, spray coating	Superhydrophilic	160.0°	99.00	–	[62]
Melamine foam-polydimethylsiloxane	One-pot emulsion polymerization	Superhydrophobic	156.8°	99.50	–	[63]
Graphitic carbon nitride/metal-organic framework-cotton	Hydrothermal, socking	Superhydrophobic	153.0°	99.00	Castor oil	[64]
Polytetrafluoroethylene @ zeolite imidazole	Electrospinning	Superhydrophobic	–	99.99	Kerosene	[65]
Zeolite mesh	Seed deposition	Superhydrophilic	–	99.98	Diesel, kerosene, rapeseed oil	[66]
Cellulose II aerogels	Lithium bromide system	Superhydrophobic	150.0°	96.00	Various oils	[67]
Lignin-cellulose aerogel	Sol-gel, freeze-drying	Superhydrophilic	–	99.00	–	[68]
FPUF@MOF-LDH@HDTMS	In-situ growth	Superhydrophobic	153.0°	99.1	–	[69]
TiO_2 cotton fabric	Immersion	Superhydrophobic	157.3°	98.4	–	[70]
Polyimide-cattail- derived active carbon aerogel	Freeze-drying and thermal imidization	Superhydrophobic	151.3°	98.3	Various oils	[71]
Melamine sponge-reduced graphene oxide- active carbon-polydimethylsiloxane	Two-step dipping	Superhydrophobic	164.0°	99.85	–	[72]
Sodium alginate-graphene oxide	–	Superhydrophilic	–	93.26	–	[73]
Polyurethane-Fe_3O_4–TiO_2	Sol-gel	Superhydrophobic	157°	90	Sunflower oil	This work

4. Conclusion

The development of effectual and viable hydrophobic materials is a crucial issue and global demand for self-cleaning materials and oily water treatment. In the current research, we described the fabrication of hydrophobic nanocomposites by sol-gel technique and using PU, Fe_2O_3 nanoparticles, Fe_3O_4 nanoparticles, and TiO_2 nanoparticles. The preparation of precursors Fe_3O_4 and TiO_2 nanoparticles were performed via co-precipitation and sol-hydrothermal methods, respectively. The synthesized nanocomposites indicated hydrophobic properties. Hydrophobic PUMNPTNP3 nanocomposite coated on the surface of filter paper possessed good oil-water separation efficiency. The present exploration will open an avenue for the design and development of materials with special wettability and the relevant utilization in self-cleaning surfaces and oil-water separation.

Author contribution statement

Asma khnadan Barani: Performed the experiments; Contributed reagents, materials, analysis tools or data.
Ghodratollah Roudini: Conceived and designed the experiments; Contributed reagents, materials, analysis tools or data.
Farahnaz Barahuie: Conceived and designed the experiments; Analyzed and interpreted the data; Contributed reagents, materials, analysis tools or data; Wrote the paper.
Siti Ujila Binti Masuri: Analyzed and interpreted the data.

Data availability statement

Data will be made available on request.

Declaration of competing interest

The authors declare that they have no known competing financial interests or personal relationships that could have appeared to influence the work reported in this paper.

References

[1] L. Tjale, H. Richards, O. Mahlangu, L.N. Nthunya, Silica nanoparticle modified polysulfone/polypropylene membrane for separation of oil-water emulsions, Results Eng. 16 (2022), 100623.
[2] A.V. Singhal, R. George, A.K. Sharma, D. Malwal, I. Lahiri, Development of superhydrophillic tannic acid-crosslinked graphene oxide membranes for efficient treatment of oil contaminated water with enhanced stability, Heliyon 6 (2020), e05127.
[3] E. Garousi, M. Hossaini Sadr, A. Rashidi, M. Yousefi, MoS2 QDs-nanoparticle-engineered based hydrophobic filter for high performance water-oil separation, Inorg. Chem. Commun. 138 (2022), 109223.
[4] B. Wang, B. Wang, Y. Zhang, S. Ma, X. Yang, Y. Feng, C. Liu, C. Shen, Superhydrophobic porous polyvinylidene fluoride monolith with outstanding environmental suitability for high-efficient continuous oil/water separation under harsh conditions, J. Environ. Chem. Eng. 10 (2022), 107480.
[5] W.E. Odiete, J.C. Agunwamba, Novel design methods for conventional oil-water separators, Heliyon 5 (2019), e01620.
[6] R. Wei, B. Yang, C. He, L. Jin, X. Zhang, C. Zhao, Versatile and robust poly(ionic liquid) coatings with intelligent superhydrophilicity/superhydrophobicity switch in high-efficient oil-water separation, Sep. Purif. Technol. 282 B (2022), 120100.
[7] F.T. Alshorifi, A.A. Alswat, R.S. Salama, Gold-selenide quantum dots supported onto cesium ferrite nanocomposites for the efficient degradation of rhodamine B, Heliyon 8 (2022), e09652.
[8] M.P. Ajith, M. Aswathi, E. Priyadarshini, P. Rajamani, Recent innovations of nanotechnology in water treatment: a comprehensive review, Bioresour. Technol. 342 (2021) 126000.
[9] S. Manikandan, R. Subbaiya, M. Saravanan, M. Ponraj, M. Selvam, A critical review of advanced nanotechnology and hybrid membrane based water recycling, reuse, and wastewater treatment processes, Chemosphere 289 (2022) 132867.
[10] J.-W. Wang, H. Abadikhah, F.-H. Wang, L.-J. Yin, X. Xu, β-silicon nitride membrane with robust inorganic-organic hybrid hydrophobic surface for water-in-oil emulsion separation, Ceram. Int. (2022), https://doi.org/10.1016/j.ceramint.2022.03.027.
[11] X. Wang, Z. Han, Y. Liu, Q. Wang, Micro-nano surface structure construction and hydrophobic modification to prepare efficient oil-water separation melamine formaldehyde foam, Appl. Surf. Sci. 505 (2020), 144577.
[12] A.A. Marcos-Fernandez, R. Navarro, E. Benito, J. Guzman, L. Garrido, Properties of polyurethanes derived from poly (diethylene glycol terephthalate), Eur. Polym. J. 155 (2021), 110576.
[13] M. Khalilifard, S. Javadian, Magnetic superhydrophobic polyurethane sponge loaded with Fe3O4@oleic acid@graphene oxide as high performance adsorbent oil from water, Chem. Eng. J. 408 (2021), 127369.
[14] J. Sarkar, Z.H. Prottoy, M.T. Bari, M.A. Al Faruque, Comparison of ANFIS and ANN modeling for predicting the water absorption behavior of polyurethane treated polyester fabric, Heliyon 7 (2021), e08000.
[15] S. Rabbani, E. Bakhshandeh, R. Jafari, G. Momen, Superhydrophobic and icephobic polyurethane coatings: fundamentals, progress, challenges and opportunities, Prog. Org. Coating 165 (2022), 106715.
[16] C.N. Matindi, M. Hu, S. Kadanyo, V.L. Quang, N.N. Gumbi, D.S. Dlamini, J. Li, Y. Hu, Z. Cui, J. Li, Tailoring the morphology of polyethersulfone/sulfonated polysulfone ultrafiltration membranes for highly efficient separation of oil-in-water emulsions using TiO2 nanoparticles, J. Membr. Sci. 620 (2021), 118868.
[17] S. Ashraf, A. Siddiqa, S. Shahida, S. Qaisar, Titanium-based nanocomposite materials for arsenic removal from water: a review, Heliyon 5 (2019), e01577.
[18] B.K. Tudu, A. Sinhamahapatra, A. Kumar, Surface modification of cotton fabric using TiO_2 nanoparticles for self-cleaning, Oil−Water separation, antistain, anti-water absorption, and antibacterial properties, ACS Omega 5 (2020) 7850–7860.
[19] M.T. Ramesan, V. Santhi, B.K. Bahuleyan, M.A. Al-Maghrabi, Structural characterization, material properties and sensor application study of in situ polymerized polypyrrole/silver doped titanium dioxide nanocomposites, Mater. Chem. Phys. 211 (2018) 343–354.
[20] T. Sampreeth, M.A. Al-Maghrabi, B.K. Bahuleyan, M.T. Ramesan, Synthesis, characterization, thermal properties, conductivity and sensor application study of polyaniline/cerium-doped titanium dioxide nanocomposites, J. Mater. Sci. 53 (2018) 591–603.
[21] B.K. Bahuleyan, C. Induja, M.T. Ramesan, Influence of titanium dioxide nanoparticles on the structural, thermal, electrical properties, and gas sensing behavior of polyaniline/phenothiazine blend nanocomposites, Polym. Compos. 40 (2019) 4416–4426.
[22] P.H. Dao, T.V. Nguyen, T.A. Nguyen, T.Y.O. Doan, T.H. Hoang, T.T. Le, P. Nguyen-Tri, Acrylic polymer/TiO_2 nanocomposite coatings: mechanism for photo-degradation and solarheat reflective recovery, Mater. Chem. Phys. 272 (2021), 124984.
[23] K. Suhailath, M.T. Ramesan, Effect of neodymium-doped titanium dioxide nanoparticles on the structural, mechanical, and electrical properties of poly (butyl methacrylate) nanocomposites, J. Vinyl Addit. Technol. 25 (2019) 9–18.
[24] N. Gu, Z. Zhang, Y. Li, Adaptive iron-based magnetic nanomaterials of high performance for biomedical applications, Nano Res. 15 (2022) 1–17.
[25] C. Baresel, V. Schaller, C. Jonasson, C. Johansson, R. Bordes, V. Chauhan, A. Sugunan, J. Sommertune, S. Welling, Functionalized magnetic particles for water treatment, Heliyon 5 (2019), e02325.
[26] T. Li, Z. Yu, T. Yang, G. Xu, Y. Guan, C. Guo, Modified Fe3O4 magnetic nanoparticles for COD removal in oil field produced water and regeneration, Environ. Technol. Innov. 23 (2021), 101630.
[27] F.S.N. Oliva, M. Sahihi, L. Lenglet, A. Ospina, E. Guenin, A. Jaramillo-Botero, W.A. Goddard, F. Bedoui, Nanoparticle size and surface chemistry effects on mechanical and physical properties of nano-reinforced polymers: the case of PVDF-Fe_3O_4 nano-composites Polym, Test 117 (2023), 107851.
[28] P. Jayakrishnan, M.T. Ramesan, Temperature dependence of the electrical conductivity of poly (Anthranilic Acid)/magnetite nanocomposites and the applicability of different conductivity models, Polym. Compos. 39 (2018) 2791–2800.
[29] H. Younes, X. Kuang, D. Lou, B. DeVries, M.M. Rahman, H. Hong, Magnetic-field-assisted DLP stereolithography for controlled production of highly aligned 3Dprinted polymer-FeO@graphene nanocomposites, Mater. Res. Bull. 154 (2022), 111938.
[30] H. Ikram, A. Al Rashid, M. Koc, Synthesis and characterization of hematite (α-Fe_2O_3) reinforced polylactic acid (PLA) nanocomposites for biomedical applications, Composites C 9 (2022), 100331.
[31] H. Aliah, D.G. Syarif, R.N. Imana, A. Sawitri, W. Darmalaksana, A. Setiawan, A. Malike, P. Gumarang, Structure analysis of nanocomposite ZnO:Fe_2O_3 based mineral yarosite as Fe_2O_3 source and its application probability, Mater. Today: Proc. 13 (2019) 36–40.
[32] N. An, L. Zhou, W. Li, X. Yuan, L. Zhao, J. Huang, Y. Zhang, H. She, L. Wang, Q. Wang, Multifunctional polymer coating cooperated with γ-Fe2O3 for boosting photoelectron-chemical water oxidation, Appl. Catal. B Environ. 318 (2022), 121869.
[33] A. Prathan, J. Sanglao, T. Wang, C. Bhoomanee, P. Ruankham, A. Gardchareon, D. Wongratanaphisan, Controlled structure and growth mechanism behind hydrothermal growth of TiO2 nanorods, Sci. Rep. 10 (2020) 8065.
[34] S.P. Schwaminger, C. Syhr, S. Berensmeier, Controlled synthesis of magnetic iron oxide nanoparticles: magnetite or maghemite, Crystals 10 (2020).
[35] C. Wang, C. Ma, C. Mu, W. Lin, Tailor-made zwitterionic polyurethane coatings: microstructure, mechanical property and their antimicrobial performance, RSC Adv. 7 (2017), 27522, https://doi.org/10.1039/C7RA04379A.
[36] M.K. Shahid, Y. Kim, Y.G. Choi, Magnetite synthesis using iron oxide waste and its application for phosphate adsorption with column and batch reactors, Chem. Eng. Res. Des. 148 (2019) 169–179.
[37] F. Barahuie, D. Dorniani, B. Saifullah, S. Gothai, M.Z. Hussein, A.K. Pandurangan, P. Arulselvan, M.E. Norhaizan, Sustained release of anticancer agent phytic acid from its chitosan-coated magnetic nanoparticles for drug-delivery system, Int. J. Nanomed. 12 (2017) 2361–2372.

[38] M.D. Purkayastha, S. Middya, J. Datta, P.P. Ray, B.D. Biswas, M. Sarkar, G.K. Darbha, N. Singh, T.P. Majumder, P. Saha, D. Das, The carrier transport properties and photodegradation ability of low temperature synthesized phase pure rutile titanium oxide nanostructured materials, Mater. Chem. Phys. 226 (2019) 362–370.

[39] N. Athir, S.A.A. Shah, F.K. Shehzad, J. Cheng, J. Zhang, L. Shi, Rutile TiO_2 integrated zwitterion polyurethane composite films as an efficient photo stable food packaging material, React. Funct. Polym. 157 (2020), 104733.

[40] P. Kongsat, K. Kudkaew, J. Tangjai, E.A. O'Rear, T. Pongprayoon, Synthesis of structure-controlled hematite nanoparticles by a surfactant-assisted hydrothermal method and property analysis, J. Phys. Chem. Solid. 148 (2021), 109685.

[41] K.M. Kim, J.H. Kim, J.H. Ahn, J.D. Kim, S. Park, K.H. Park, J.M. Lee, Synthesis of nanoparticle-enhanced polyurethane foams and evaluation of mechanical characteristics, Compos. B Eng. 136 (2018) 28–38.

[42] W. Xiao, F. Jiao, H. Zhao, W. Qin, G. Qiu, J. Wang, Adsorption structure and mechanism of styryl phosphoric acid at the rutile–water interface, Minerals 8 (2018) 360.

[43] M. Tadic, D. Trpkov, L. Kopanja, S. Vojnovic, M. Panjan, Hydrothermal synthesis of hematite (a-Fe2O3) nanoparticle forms: synthesis conditions, structure, particle shape analysis, cytotoxicity and magnetic properties, J. Alloys Compd. 792 (2019) 599–609.

[44] X. Zhou, Q. Huang, S. Xu, Z. Fan, Pore structure and adsorption properties of welan gum modified polyurethane, Mater. Res. Express 6 (2019), 095316.

[45] T. Boulaouche, D.B. Kherroub, A. Benzerafa, K. Khimeche, M. Belbachir, New synthesis of polyurethane nanocomposites based on maghnite used both as a catalyst and as an inorganic improver of thermal, mechanical and textural properties, J. Mater. Res. Technol. 9 (2020) 15222–15232.

[46] S.M. Moatmed, M.H. Khedr, S.I. El-dek, H.-Y. Kim, A.G. El-Deen, Highly efficient and reusable superhydrophobic/superoleophilic polystyrene@ Fe_3O_4 nanofiber membrane for high-performance oil/water separation, J. Environ. Chem. Eng. 7 (2019), 103508.

[47] S.M. Kong, Y. Han, N.-I. Won, Y.H. Na, Polyurethane sponge with a modified specific surface for repeatable oil−water separation, ACS Omega 6 (2021), 33969−33975.

[48] S. Mohammed Hailan, D. Ponnamma, I. Krupa, The separation of oil/water mixtures by modified melamine and polyurethane foams: a review, Polymer 13 (2021) 4142.

[49] H. Li, S. Lin, X. Feng, Q. Pan, Preparation of superhydrophobic and superoleophilic polyurethane foam for oil spill cleanup, J. Macromol. Sci. 58 (2021) 758–768.

[50] J. Meng, F. Li, T. Li, W. Cao, Coating polyurethane sponge with Dy-MOF for efficient oil–water separation in complex environments, Appl. Surf. Sci. 614 (2023), 156183.

[51] M. Satria, T.A. Saleh, Synthesis of superhydrophobic/superoleophilic stearic acid and polymer-modified magnetic polyurethane for oil-water separation: effect of polymeric nature, J. Colloid Interface Sci. 629 (2023) 522–534.

[52] M. Wu, R. An, S.K. Yadav, X. Jiang, Graphene tailored by Fe_3O_4 nanoparticles: low adhesive and durable superhydrophobic coatings, RSC Adv. 9 (2019), 16235.

[53] R. Sun, L. He, Q. Shang, S. Jiang, C. Zhou, P. Hong, H. Zhao, S. Sun, C. Li, Hydrophobic magnetic porous material of Eichhornia Crassipes for highly efficient oil adsorption and separation, ACS Omega 5 (2020) 9920–9928.

[54] S. Shamsudin, M.K. Ahmad, A.N. Aziz, R. Fakhriah, F. Mohamad, N. Ahmad, N. Nafarizal, C.F. Soon, A.S. Ameruddin, A.B. Faridah, M. Shimomura, K. Murakami, Hydrophobic rutile phase TiO_2 nanostructure and its properties for self-cleaning application, AIP Conf. Proc. 1883 (2017), 020030. AIP Publishing LLC.

[55] B.K. Tudu, A. Sinhamahapatra, A. Kumar, Surface modification of cotton fabric using TiO2 nanoparticles for self-cleaning, oil−water separation, antistain, anti-water absorption, and antibacterial properties, ACS Omega 5 (2020) 7850–7860.

[56] Z. Li, L. Yin, S. Jiang, L. Chen, S. Sang, H. Zhang, A photocatalytic degradation self-cleaning composite membrane for oil-water separation inspired by light-trapping effect of moth-eye, J. Membr. Sci. 669 (2023), 121337.

[57] J. Bang, S. Park, S.-W. Hwang, J.-K. Oh, H. Yeo, H.-J. Jin, H.W. Kwak, Biodegradable and hydrophobic nanofibrous membranes produced by solution blow spinning for efficient oil/water separation, Chemosphere 312 (2023), 137240.

[58] S. Tang, S. Sun, T. Liu, M. Li, Y. Jiang, D. Wang, N. Guo, Z. Guo, X. Chang, Bionic engineering-induced formation of hierarchical structured minerals with superwetting surfaces for oil-water separation, J. Membr. Sci. 669 (2023), 121261.

[59] Y. Wang, F. Meng, L. Han, X. Liu, F. Guo, H. Lu, D. Cheng, W. Wang, Constructing a highly tough, durable, and renewable flexible filter by epitaxial growth of a glass fiber fabric for high flux and superefficient oil-water separation, J. Hazard Mater. (2023), 130807.

[60] Z. Li, M. Wang, Y. Li, J. Ren, C. Pei, Effect of cellulose nanocrystals on bacterial cellulose hydrogel for oil-water separation, Sep. Purif. Technol. 304 (2023), 122349.

[61] W. Chen, H. Wang, W. Lan, A. Zhang, C. Liu, Fabrication of sugarcane bagasse ester-based porous nanofiber membrane by electrospinning for efficient oil-water separation, Ind. Crop. Prod. 187 (2022), 115480.

[62] U. Baig, M.A. Dastageer, M.A. Gondal, Facile fabrication of super-wettable mesh membrane using locally-synthesized cobalt oxide nanoparticles and their application in efficient gravity driven oil/water separation, Colloids Surf. A: Physicochem. Eng. Asp. 660 (2023), 130793.

[63] H. Huang, C. Zhao, J. Li, J. Cheng, D. Xiang, J. Wei, Y. Yang, Z. Li, Y. Li, M. Qin, Y. Wu, Facile preparation of superhydrophobic melamine foam via one-pot emulsion polymerization for efficient oil/water separation, Colloids Surf. A: Physicochem. Eng. Asp. 658 (2023), 130710.

[64] H. Wang, J. Meng, F. Li, T. Li, Graphitic carbon nitride/metal-organic framework composite functionalized cotton for efficient oil-water separation and dye degradation, J. Clean. Prod. 385 (2023), 135758.

[65] Y. Li, T. Fan, W. Cui, X. Wang, S. Ramakrishna, Y. Long, Harsh environment-tolerant and robust PTFE@ZIF-8 fibrous membrane for efficient photocatalytic organic pollutants degradation and oil/water separation, Sep. Purif. Technol. 306 (2023), 122586.

[66] L. Cao, J. Zhou, H. Hao, P.K. Dutta, High-flux, efficient and reusable zeolite/stainless steel meshes for oil/water separation, Microporous Mesoporous Mater. 336 (2022), 111870.

[67] Z. Ma, Y. Han, X. Xing, H. Zhu, Q. Wang, X. Wang, Highly efficient oil–water separation of superhydrophobic cellulose II aerogel based on dissolution and regeneration of cotton in lithium bromide system, J. Mol. Liq. 367 (2022), 120543.

[68] Z. Tan, L. Hu, D. Yang, D. Zheng, X. Qiu, Lignin: excellent hydrogel swelling promoter used in cellulose aerogel for efficient oil/water separation, J. Colloid Interface Sci. 629 (2023) 422–433.

[69] J. Piao, M. Lu, J. Ren, Y. Wang, T. Feng, Y. Wang, C. Jiao, X. Chen, S. Kuang, MOF-derived LDH modified flame-retardant polyurethane sponge for high-performance oil-water separation: interface engineering design based on bioinspiration, J. Hazard Mater. 444 (2023), 130398.

[70] J. Yang, T. He, X. Li, R. Wang, S. Wang, Y. Zhao, H. Wang, Rapid dipping preparation of superhydrophobic TiO_2 cotton fabric for multifunctional highly efficient oil-water separation and photocatalytic degradation, Colloids Surf. A: Physicochem. Eng. Asp. 657 (2023), 130590.

[71] Y. Wang, X. Zeng, W. Wang, P. Zhou, R. Zhang, H. Chen, G. Liu, Superhydrophobic polyimide/cattail-derived active carbon composite aerogels for effective oil/water separation, Sep. Purif. Technol. 308 (2023), 122994.

[72] M. Yang, L. Yang, Z. Chen, Y. Ding, M. Li, Q. Wu, T. Liu, L. Liu, Superhydrophobic/superoleophilic modified melamine sponge for oil/water separation, Ceram. Int. (2023), https://doi.org/10.1016/j.ceramint.2022.12.001.

[73] M. Ehsan, H. Razzaq, S. Razzaque, M. Kanwal, I. Hussain, Engineering nanocomposite membranes of sodium alginate-graphene oxide for efficient separation of oil-water and antifouling performance, J. Environ. Chem. Eng. 11 (2023), 109185.